ChemComm

COMMUNICATION

View Article Online
View Journal | View Issue

Cite this: *Chem. Commun.*, 2024, **60**, 3669

Received 28th November 2023,
Accepted 27th February 2024

DOI: 10.1039/d3cc05821b

rsc.li/chemcomm

Utilisation of carbon dioxide and nitrate for urea electrosynthesis with a Cu-based metal–organic framework†

Meng-Di Zhang,‡[a] Jia-Run Huang,‡[a] Pei-Qin Liao *[a] and Xiao-Ming Chen *[ab]

It is important and challenging to utilise CO_2 and NO_3^- as a feedstock for electrosynthesis of urea. Herein, we reported a stable 2D metal–organic framework (MOF) Cu-HATNA, possessing planar CuO_4 active sites, as an efficient electrocatalyst for coupling CO_2 and NO_3^- into urea, achieving a high yield rate of 1.46 g h^{-1} g_{cat}^{-1} with a current density of 44.2 mA cm^{-1} at −0.6 V *vs.* RHE. This performance surpasses most of the previously reported catalysts, revealing the great prospects of MOFs in sustainable urea synthesis.

Urea is an indispensable nitrogen fertiliser that greatly supports global agriculture and serves as a vital raw material to produce pharmaceuticals and diverse chemical compounds.[1–5] The dominant industrial method for the synthesis of urea is the Bosch–Meiser process ($2NH_3 + CO_2 \rightarrow CO(NH_2)_2 + H_2O$), typically conducted under high-temperature and high-pressure conditions (*e.g.*, 150–200 °C, 150–250 bar).[5–9] Such a process is energy-intensive, consuming nearly 80% of the world's annual production of NH_3.[3,10–12] Given the importance of a sustainable economy, developing an energy-saving and efficient method for urea synthesis is crucial.

Recent advancements have sparked interest in the electrosynthesis of urea *via* the utilisation of CO_2 and NO_3^-.[1,6,8] This approach has been considered as a viable route to achieve direct urea synthesis at ambient temperature and atmospheric pressure, offering an alternative to the conventional urea manufacture.[5,8,10,11,13,14] To date, precious and non-precious metal-based electrocatalysts have been developed and explored for C–N coupling to synthesize urea from CO_2 and NO_3^-, exhibiting impressive electrocatalytic performances.[2–6,10–12,15] For example, Chen *et al.* used Fe(a)@C–Fe_3O_4/CNTs containing dual Fe-based active sites as a catalyst to electrochemically couple CO_2 and NO_3^- into urea, achieving an average yield rate of 1.34 ± 0.11 g h^{-1} g_{cat}^{-1} at −0.65 V *vs.* reversible hydrogen electrode (RHE).[4] Yu *et al.* reported an $In(OH)_3$–S catalyst with single {100} facets, achieving urea synthesis from CO_2 and NO_3^- with a yield rate of 0.53 g h^{-1} g_{cat}^{-1} at −0.6 V *vs.* RHE.[12] Despite these advancements, this catalytic process confronts substantial challenges, including the individual electroreduction of CO_2 and NO_3^-, as well as the unavoidable hydrogen evolution reaction (HER).[1,2,8,11,13] Therefore, there is a strong expectation to advance the development of more efficient electrocatalysts for further improving the performance of urea electrosynthesis.

Copper-based catalysts have demonstrated excellent electrocatalytic activity in both the electrochemical CO_2 reduction reaction (CO_2RR)[16–21] and NO_3^- reduction reaction (NO_3RR).[22–26] This suggests the capacity to activate CO_2 and NO_3^- species, thus potentially enabling C–N coupling reactions crucial for urea synthesis. Up to now, several Cu-based materials have been investigated for the electrosynthesis of urea,[2,5,6,8] but there remains scope for improving their performance. Metal–organic frameworks (MOFs) are a class of materials with crystalline porous structures and periodically arranged active sites. These characteristics render MOFs highly promising for achieving both high current density and selectivity in electrocatalysis.[27–31] Hence, Cu-based MOF catalysts can be expected to exhibit excellent activity in the electrosynthesis of urea. As shown in Fig. 1a, **Cu-HATNA** (HATNA–6OH = diquinoxalino[2,3-*a*:2′,3′-*c*]phenazine-2,3,8,9,14,15-hexol) is a hexagonal two-dimensional (2D) MOF constructed by tripodal bridging HATNA–6OH ligands and planar CuO_4 nodes.[32] Although previous studies have demonstrated the high redox activity of CuO_4, research on using Cu-based catalysts for the electrosynthesis of urea remains rare to date. In this work, we explore **Cu-HATNA** as a catalyst and elucidate its unique mechanism in urea synthesis, which offers a new perspective for optimizing urea electrosynthesis and possesses practical application potential in this field.

Solvothermal reaction of HATNA–6OH (Fig. S1, ESI†) and copper nitrate hemipentahydrate at 85 °C gave the black

[a] *MOE Key Laboratory of Bioinorganic and Synthetic Chemistry, GBRCE for Functional Molecular Engineering, School of Chemistry, IGCME, Sun Yat-Sen University, Guangzhou, 510275, China. E-mail: liaopq3@mail.sysu.edu.cn, cxm@mail.sysu.edu.cn*

[b] *Chemistry and Chemical Engineering Guangdong Laboratory, Shantou, 515031, China*

† Electronic supplementary information (ESI) available. See DOI: https://doi.org/10.1039/d3cc05821b

‡ These authors contributed equally.

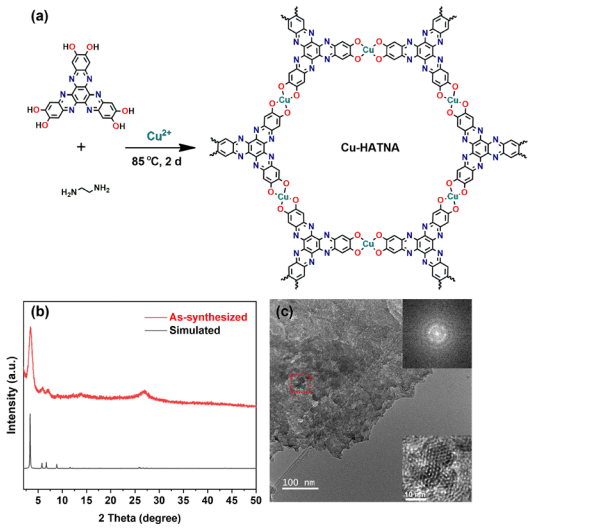

Fig. 1 (a) Illustration of the synthesis of **Cu-HATNA**. (b) Experimental and simulated PXRD patterns of **Cu-HATNA**. (c) AC-TEM image of **Cu-HATNA** (inset in c: selected area electron diffraction image and the related FFT analysis).

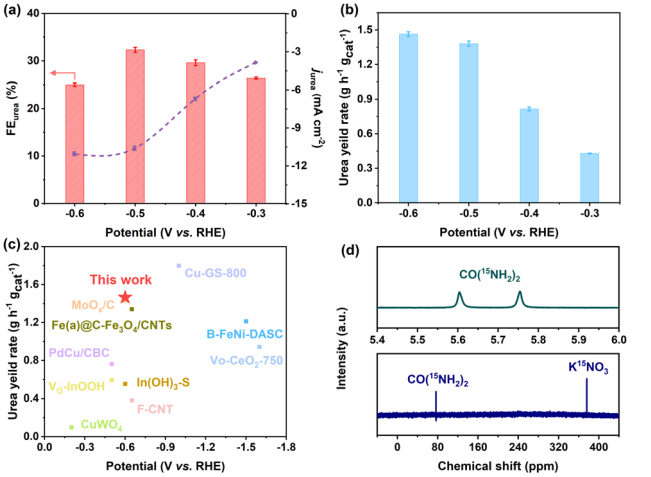

Fig. 2 Electrochemical performances of **Cu-HATNA**. (a) FEs and partial current densities of urea at different potentials. (b) Urea yield rates at different potentials. (c) Comparison of the urea yield rates between **Cu-HATNA** and the reported catalysts. (d) ^{1}H NMR and ^{15}N NMR spectra of 0.1 M $KHCO_3$ + 0.1 M $K^{15}NO_3$ electrolyte for isotope labelling measurements.

microcrystalline powder of **Cu-HATNA**. Its purity was confirmed by the powder X-ray diffraction (PXRD) pattern (Fig. 1b). Scanning electron microscopy (SEM) images in Fig. S2 (ESI†) displayed the stacked sheet-like morphology of **Cu-HATNA**. Aberration corrected transmission electron microscopy (AC-TEM) provided direct visualisation of hexagonal channels (Fig. 1c), which is consistent with the crystal structure. Inductively coupled plasma atomic emission spectroscopy (ICP-AES), energy-dispersive X-ray (EDX) spectroscopy (Fig. S3 and S4b, ESI†) and X-ray photoelectron spectroscopy (XPS) spectra (Fig. S5, ESI†) revealed the uniform distribution of C, N, O and Cu elements over the whole structure. The high-resolution XPS spectrum of the Cu 2p region (Fig. S6, ESI†) and Cu LMM Auger spectrum (Fig. S7, ESI†) suggested a mixed state of Cu(I) and Cu(II) in the CuO_4 nodes. The thermogravimetric curve indicated that the thermal stability of **Cu-HATNA** is up to 300 °C (Fig. S8, ESI†).

The urea synthesis performance of **Cu-HATNA** by coupling NO_3^- and CO_2 was evaluated using a flow-cell with a typical three-electrode system. The as-synthesised **Cu-HATNA** was uniformly coated on a gas diffusion layer (GDL) with Nafion binder to fabricate the working electrode. During the electrochemical measurements, high-purity CO_2 was streamed to the cathode with a constant flow rate of 30 mL min^{-1} and 0.1 M $KHCO_3$ + 0.1 M KNO_3 solution was used as the electrolyte circulating through the cathodic and anodic compartments in the reactor. Firstly, linear sweep voltammetry (LSV) was recorded at 10 mV s^{-1} to preliminarily investigate the electrocatalytic activity of the sample. As displayed in the LSV curve (Fig. S9, ESI†), the current density increased significantly at applied potentials from 0 to −0.6 V *vs.* RHE, implying that **Cu-HATNA** has good activity for electrocatalytic urea synthesis. The chronoamperometry tests were conducted at the potentials of −0.3 to −0.6 V *vs.* RHE (Fig. S10, ESI†) and the electrolyte at each potential was spectrophotometrically analysed after pretreatment with the diacetyl monoxime method to quantify the produced urea (Fig. S11 and S12, ESI†). It can be seen that with increasing applied potential, the faradaic efficiency (FE) of urea increased, reaching a maximum value of 32.3% at −0.5 V *vs.* RHE (Fig. 2a). Although the selectivity towards urea gradually declined as the potential became more negative, the **Cu-HATNA** catalyst provided the largest partial current density of 11 mA cm^{-2} for urea production at the potential of −0.6 V *vs.* RHE (Fig. 2a). At the same potential, **Cu-HATNA** exhibited the highest urea yield rate of 1.46 g h^{-1} g_{cat}^{-1} (Fig. 2b), which is superior to most of the recently reported catalysts for electrosynthesis of urea (Fig. 2c and Table S1, ESI†). As shown in Fig. 2d, the ^{1}H nuclear magnetic resonance (NMR) spectrum of the electrolyte with $K^{15}NO_3$ revealed the typical doublet coupling of $CO(^{15}NH_2)_2$ and the typical $CO(^{15}NH_2)_2$ peak at 76.8 ppm was observed in the ^{15}N NMR spectrum, demonstrating that the NO_3^- ion was the nitrogen source of the produced urea. Furthermore, there was no detectable signal of urea in the ^{1}H NMR spectra when the electrochemical test was performed without the presence of CO_2 + $KHCO_3$ or KNO_3, further confirming that the urea was indeed derived from the C–N coupling reaction by **Cu-HATNA**.

The stability test of **Cu-HATNA** was then conducted at a given potential of −0.5 V *vs.* RHE. As shown in Fig. S13 (ESI†), the current density was well maintained without any significant degradation over the course of 10 hours of operation. Besides, SEM (Fig. S14, ESI†), AC-TEM (Fig. S15, ESI†) images and PXRD patterns (Fig. S16, ESI†) indicated that the morphology and crystalline framework structure of **Cu-HATNA** remained almost unchanged and there was no obvious Cu or Cu oxide formed from **Cu-HATNA** after electrocatalysis. The XPS profiles showed negligible changes of Cu species after testing (Fig. S17 and S18, ESI†). More importantly, the analysis of the X-ray absorption spectra (XA-S) (Fig. 3 and Table S2, ESI†) indicated that the Cu

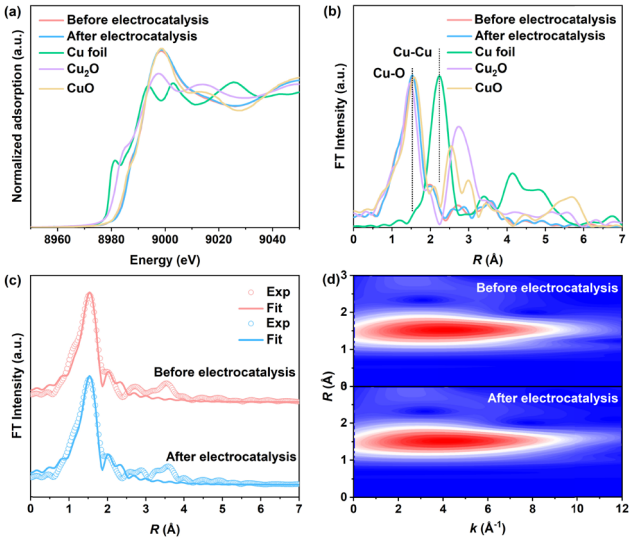

Fig. 3 (a) Cu K-edge XANES spectra and (b) FT-EXAFS spectra of **Cu-HATNA** before and after electrocatalysis, Cu foil, Cu_2O and CuO. (c) Cu K-edge spectra of EXAFS fitting for **Cu-HATNA** before and after electrocatalysis. (d) WT-EXAFS spectra of **Cu-HATNA** before and after electrocatalysis.

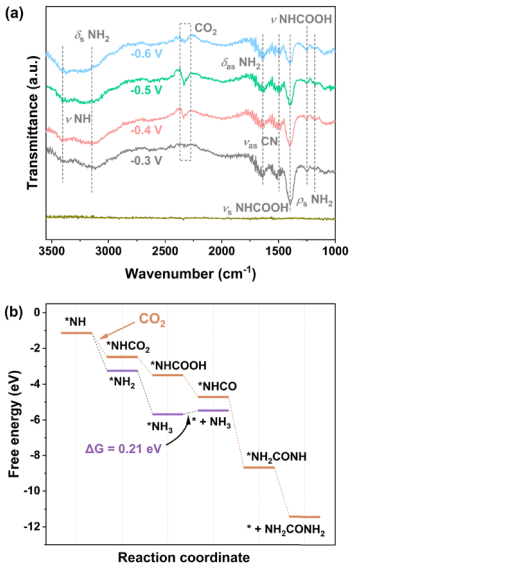

Fig. 4 (a) *Operando* ATR-FTIR spectra measurements under various potentials for the **Cu-HATNA** in 0.1 M $KHCO_3$ + 0.1 M KNO_3 electrolyte. (b) Free energy diagram for urea formation on **Cu-HATNA**.

node in **Cu-HATNA** is coordinated with four O atoms, and the coordination environment of the sample before and after electrolysis remained basically the same. The above results suggest that **Cu-HATNA** possesses good electrochemical and structural stability for urea synthesis.

Operando electrochemical attenuated total reflection Fourier transform infrared spectroscopy (ATR-FTIR) was performed to determine the generated intermediate species during the urea synthesis process. The infrared signals were collected within the potential range from −0.3 to −0.6 V *vs.* RHE under electrochemical conditions (Fig. 4a). The peaks at about 1250 and 1397 cm^{-1} originate from the OH-deformation and symmetric stretching of the *NHCOOH intermediate.[1,12,33] The emergence of the peaks located at 1182, 1639, 3148 and 3407 cm^{-1} confirmed the formation of urea, which can be assigned to the rocking, asymmetric bending, symmetric bending of $-NH_2$ and stretching of N–H, respectively.[1,12,15,34] The asymmetric stretching of C–N at 1495 cm^{-1} can also be observed, further testifying that the C–N coupling was successfully realised.[1] Notably, as the negative applied potential increases, the signal intensity related to $-NH_2$ gradually enhanced, which is in good accordance with the electrocatalysis results.

Guided by the ATR-FTIR results, density functional theory (DFT) calculations were carried out to elucidate the possible reaction pathways involved in the electrosynthesis of urea by **Cu-HATNA**. Initially, the reduction steps of the CO_2RR and NO_3RR were individually assessed. It was found that a high reaction-free energy of 1.57 eV is required for the conversion of CO_2 to the *COOH intermediate, which is the potential limiting step (PLS) of CO_2RR (Fig. S20, ESI†). In contrast, the reduction of NO_3^- to *NO *via* a series of reactions ($HNO_3^- + 3H^+ + 4e^- \rightarrow$ *NO + $2H_2O$) occurs spontaneously. Subsequently, the *NO can be further reduced to an *NH intermediate with the reaction-free energy of only 0.56 eV. This means that the PLS of the NO_3RR (0.56 eV) is much lower than that of the CO_2RR (1.57 eV), indicating the relative ease of reducing NO_3^- on **Cu-HATNA** as opposed to CO_2. Interestingly, the *NH intermediate is so strongly alkaline that it could spontaneously react with either a CO_2 molecule or proton to generate the *$NHCO_2$ or *NH_2 intermediate (Fig. 4b). However, plagued by challenges in NH_3 desorption (ΔG = 0.21 eV), the *NH intermediate predominantly forms a *$NHCO_2$ intermediate with a reaction-free energy of −1.33 eV. This intermediate was further reduced to *NHCO, which then reacted with *NH_2 (derived from the NO_3RR) to generate the *$NHCONO_2$ intermediate. Finally, the intermediate *$NHCONO_2$ was further reduced into urea. Consequently, the whole reaction mechanism is proposed in Fig. 4b. Overall, the high-performance of urea electrosynthesis on **Cu-HATNA** can be attributed to the high efficacy of its planar CuO_4 active sites in generating the key intermediate *NH, thereby facilitating the C−N coupling to yield urea.

In summary, the Cu-based MOF **Cu-HATNA** with CuO_4 active sites achieves high-performance towards electrosynthesis of urea through utilisation of CO_2 and NO_3^- as a feedstock. As revealed by our mechanism study, the CuO_4 sites also have high activity for the electrosynthesis of urea in addition to the CO_2RR. This work demonstrated the tremendous potential of Cu-based electrocatalysts, which is expected to help in the design and development of efficient electrocatalysts for direct urea synthesis.

This work was supported by the National Key Research and Development Program of China (2021YFA1500401), NSFC (21890380 and 21821003), Science and Technology Innovation Special Support Project of Guangdong Province, China (STKJ2023078), Science and Technology Key Project of Guangdong Province, China (2020B010188002).

Conflicts of interest

There are no conflicts to declare.

Notes and references

1 M. Jiang, M. Zhu, M. Wang, Y. He, X. Luo, C. Wu, L. Zhang and Z. Jin, *ACS Nano*, 2023, **17**, 3209–3224.
2 J. Leverett, T. Tran-Phu, J. A. Yuwono, P. Kumar, C. Kim, Q. Zhai, C. Han, J. Qu, J. Cairney, A. N. Simonov, R. K. Hocking, L. Dai, R. Daiyan and R. Amal, *Adv. Energy Mater.*, 2022, **12**, 2201500.
3 C. Lv, C. Lee, L. Zhong, H. Liu, J. Liu, L. Yang, C. Yan, W. Yu, H. H. Hng, Z. Qi, L. Song, S. Li, K. P. Loh, Q. Yan and G. Yu, *ACS Nano*, 2022, **16**, 8213–8222.
4 J. Geng, S. Ji, M. Jin, C. Zhang, M. Xu, G. Wang, C. Liang and H. Zhang, *Angew. Chem., Int. Ed.*, 2023, **62**, e202210958.
5 S. Zhang, J. Geng, Z. Zhao, M. Jin, W. Li, Y. Ye, K. Li, G. Wang, Y. Zhang, H. Yin, H. Zhang and H. Zhao, *EES Catal.*, 2023, **1**, 45–53.
6 Y. Zhao, Y. Ding, W. Li, C. Liu, Y. Li, Z. Zhao, Y. Shan, F. Li, L. Sun and F. Li, *Nat. Commun.*, 2023, **14**, 4491.
7 J. Qin, N. Liu, L. Chen, K. Wu, Q. Zhao, B. Liu and Z. Ye, *ACS Sustainable Chem. Eng.*, 2022, **10**, 15869–15875.
8 Q. Zhao, X. Lu, Y. Wang, S. Zhu, Y. Liu, F. Xiao, S. X. Dou, W.-H. Lai and M. Shao, *Angew. Chem., Int. Ed.*, 2023, **62**, e202307123.
9 X. Liu, P. V. Kumar, Q. Chen, L. Zhao, F. Ye, X. Ma, D. Liu, X. Chen, L. Dai and C. Hu, *Appl. Catal., B*, 2022, **316**, 121618.
10 X. Wei, X. Wen, Y. Liu, C. Chen, C. Xie, D. Wang, M. Qiu, N. He, P. Zhou, W. Chen, J. Cheng, H. Lin, J. Jia, X.-Z. Fu and S. Wang, *J. Am. Chem. Soc.*, 2022, **144**, 11530–11535.
11 X. Zhang, X. Zhu, S. Bo, C. Chen, M. Qiu, X. Wei, N. He, C. Xie, W. Chen, J. Zheng, P. Chen, S. P. Jiang, Y. Li, Q. Liu and S. Wang, *Nat. Commun.*, 2022, **13**, 5337.
12 C. Lv, L. Zhong, H. Liu, Z. Fang, C. Yan, M. Chen, Y. Kong, C. Lee, D. Liu, S. Li, J. Liu, L. Song, G. Chen, Q. Yan and G. Yu, *Nat. Sustainability*, 2021, **4**, 868–876.
13 S. Liu, M. Wang, Q. Cheng, Y. He, J. Ni, J. Liu, C. Yan and T. Qian, *ACS Nano*, 2022, **16**, 17911–17930.
14 J. Li, Y. Zhang, K. Kuruvinashetti and N. Kornienko, *Nat. Rev. Chem.*, 2022, **6**, 303–319.
15 M. Sun, G. Wu, J. Jiang, Y. Yang, A. Du, L. Dai, X. Mao and Q. Qin, *Angew. Chem., Int. Ed.*, 2023, **62**, e202301957.
16 X.-F. Qiu, H.-L. Zhu, J.-R. Huang, P.-Q. Liao and X.-M. Chen, *J. Am. Chem. Soc.*, 2021, **143**, 7242–7246.
17 D.-L. Meng, M.-D. Zhang, D.-H. Si, M.-J. Mao, Y. Hou, Y.-B. Huang and R. Cao, *Angew. Chem., Int. Ed.*, 2021, **60**, 25485–25492.
18 Z.-H. Zhao, K. Zheng, N.-Y. Huang, H.-L. Zhu, J.-R. Huang, P.-Q. Liao and X.-M. Chen, *Chem. Commun.*, 2021, **57**, 12764–12767.
19 M. Zhang, M. Lu, M.-Y. Yang, J.-P. Liao, Y.-F. Liu, H.-J. Yan, J.-N. Chang, T.-Y. Yu, S.-L. Li and Y.-Q. Lan, *eScience*, 2023, **3**, 100116.
20 H.-L. Zhu, H.-Y. Chen, Y.-X. Han, Z.-H. Zhao, P.-Q. Liao and X.-M. Chen, *J. Am. Chem. Soc.*, 2022, **144**, 13319–13326.
21 Z.-H. Zhao, H.-L. Zhu, J.-R. Huang, P.-Q. Liao and X.-M. Chen, *ACS Catal.*, 2022, **12**, 7986–7993.
22 H. Liu, X. Lang, C. Zhu, J. Timoshenko, M. Rüscher, L. Bai, N. Guijarro, H. Yin, Y. Peng, J. Li, Z. Liu, W. Wang, B. R. Cuenya and J. Luo, *Angew. Chem., Int. Ed.*, 2022, **61**, e202202556.
23 P. Li, R. Li, Y. Liu, M. Xie, Z. Jin and G. Yu, *J. Am. Chem. Soc.*, 2023, **145**, 6471–6479.
24 Y. Wang, W. Zhou, R. Jia, Y. Yu and B. Zhang, *Angew. Chem., Int. Ed.*, 2020, **59**, 5350–5354.
25 G.-F. Chen, Y. Yuan, H. Jiang, S.-Y. Ren, L.-X. Ding, L. Ma, T. Wu, J. Lu and H. Wang, *Nat. Energy*, 2020, **5**, 605–613.
26 Y. Wang, A. Xu, Z. Wang, L. Huang, J. Li, F. Li, J. Wicks, M. Luo, D.-H. Nam, C.-S. Tan, Y. Ding, J. Wu, Y. Lum, C.-T. Dinh, D. Sinton, G. Zheng and E. H. Sargent, *J. Am. Chem. Soc.*, 2020, **142** 5702–5708.
27 L. Jiao, Y. Wang, H.-L. Jiang and Q. Xu, *Adv. Mater.*, 2018, **30**, 1703663.
28 L. S. Xie, G. Skorupskii and M. Dincă, *Chem. Rev.*, 2020, **120**, 8536–8580.
29 R. Freund, O. Zaremba, G. Arnauts, R. Ameloot, G. Skorupskii, M. Dincă, A. Bavykina, J. Gascon, A. Ejsmont, J. Goscianska, M. Kalmutzki, U. Lächelt, E. Ploetz, C. S. Diercks and S. Wuttke, *Angew. Chem., Int. Ed.*, 2021, **60**, 23975–24001.
30 S.-L. Li and Q. Xu, *Energy Environ. Sci.*, 2013, **6**, 1656–1683.
31 B. Li, H.-M. Wen, Y. Cui, W. Zhou, G. Qian and B. Chen, *Adv. Mater.*, 2016, **28**, 8819–8860.
32 Y. Liu, S. Li, L. Dai, J. Li, J. Lv, Z. Zhu, A. Yin, P. Li and B. Wang, *Angew. Chem., Int. Ed.*, 2021, **60**, 16409–16415.
33 N. J. Firet and W. A. Smith, *ACS Catal.*, 2017, **7**, 606–612.
34 C. Chen, X. Zhu, X. Wen, Y. Zhou, L. Zhou, H. Li, L. Tao, Q. Li, S. Du, T. Liu, D. Yan, C. Xie, Y. Zou, Y. Wang, R. Chen, J. Huo, Y. Li, J. Cheng, H. Su, X. Zhao, W. Cheng, Q. Liu, H. Lin, J. Luo, J. Chen, M. Dong, K. Cheng, C. Li and S. Wang, *Nat. Chem.*, 2020, **12**, 717–724.

